



Fluorometric dopamine assay based on an energy transfer system composed of aptamer-functionalized MoS₂ quantum dots and MoS₂ nanosheets

Jia Chen^{1,2} · Yunchun Li¹ · Yanni Huang¹ · Haijuan Zhang¹ · Xingguo Chen³ · Hongdeng Qiu¹

Received: 8 September 2018 / Accepted: 2 December 2018 / Published online: 7 January 2019
© Springer-Verlag GmbH Austria, part of Springer Nature 2019

Abstract

The authors describe a fluorometric strategy for the determination of dopamine (DA). It is based on the use of aptamer-functionalized MoS₂ quantum dots (QDs) and MoS₂ nanosheets (NSs). The QDs and NSs were extensively characterized with regard to their physical and chemical properties using methods such as TEM, XRD, FT-IR, EDX and molecular spectroscopies. The aptamer against dopamine was labeled with QDs acting as the energy donor in an energy transfer system, while the NSs serve as the energy acceptor. Under the optimal conditions, the fluorescence (FL) intensity (best measured at excitation/emission peaks of 315/412 nm) increases with increasing DA concentration in the range from 0.1 nM to 1000 nM, with a lower detection limit of 45 pM. The method was successfully applied to the determination of DA in complex matrices. In our perception, the method has a wide scope in that it may be extended to other biomolecules for which respective aptamer are available. The QDs show excellent optical properties, good stability, low cytotoxicity, and may also be applied to fluorometric imaging of live cells.

Keywords Nanomaterial · Fluorescence resonance energy transfer (FRET) · Neurotransmitter · Aptasensor · Turn-on · Bioassay · Static quenching

Introduction

Aptamers are artificial, ssDNA or RNA sequences, which are selected from random-sequence nucleic acids libraries [1, 2]. They have the ability to bind, with high affinity and specificity, to various kind of targets including small organic

molecules, proteins, metal ions, intact virus or cells [3–5]. In addition, they are thermally stable, economical, reusable, low toxic, and exhibit excellently stability during long-term storage. Based on the above outstanding property, it is not surprising that aptamer bound onto the surface of nanomaterial are now being widely applied to construct various biosensing platforms [6–8].

However, most of the above-mentioned studies were mainly based on turn-off FL sensors, which had low detection sensitivity owing to strong matrix effects [9]. Therefore, a new kind of biosensing technology based on turn-on mechanism is urgently required to improve the sensitivity.

Molybdenum disulfide (MoS₂) has garnered tremendous research interest in scientific community due to its excellent solubility, easy exploitation without the extra treatment with acids and oxidative reagents [10, 11]. This material consists of atomic layers of sulfur-molybdenum-sulfur stacked together via van der Waals (vdW) interactions [12]. Apart from the use of MoS₂ as a catalyst for hydro desulfurization and electrochemical hydrogen evolution reaction (HER), hydrogen storage, transistors, nano-lubrication and batteries [13]. Two-dimensional MoS₂ nanosheets (NSs) and zero-dimensional

Electronic supplementary material The online version of this article (<https://doi.org/10.1007/s00604-018-3143-5>) contains supplementary material, which is available to authorized users.

✉ Hongdeng Qiu
hdqiu@licp.cas.cn

- ¹ CAS Key Laboratory of Chemistry of Northwestern Plant Resources and Key Laboratory for Natural Medicine of Gansu Province, Lanzhou Institute of Chemical Physics, Chinese Academy of Sciences, Lanzhou 730000, China
- ² Chinese Academy of Sciences, University of Chinese Academy of Sciences, Beijing 100039, China
- ³ State Key Laboratory of Applied Organic Chemistry, Lanzhou University, Lanzhou 730000, China

MoS₂ quantum dots (QDs) also have been widely used in fluorescence (FL) sensing, biomedical imaging, drug delivery, etc. [14, 15]. In 2013, Zhang et al. firstly reported that NSs were able to spontaneously adsorb single-stranded DNA by the van der Waals interaction between nucleobases and the basal plane of NSs but hardly interact with rigid double-stranded DNA. NSs are known to quench the FL of the dye [16]. After that, NSs based various fluorescent sensing platforms have been widely used [17–19]. If the lateral size of single layer NSs is reduced to less than 10 nm (this leading to monolayer QDs), new quantum confinement effects can be observed such as bright FL, but also good stability, water solubility, low toxicity, and biocompatibility [20, 21]. However, the turn-on fluorometric biosensor with QDs as energy donor and NSs as energy acceptor for the determination of biomolecules has not been explored.

Inspired by all above facts, we present the first example of application of QDs and NSs for the construction of a versatile turn-on fluorescent aptasensor. Dopamine (DA) was used as a model analyte. DA is a neurotransmitter that plays a critical role in the function of the cardiovascular and endocrine system as well as central nervous system. Some important nervous system diseases are associated with dysfunctions of DA, including schizophrenia, Parkinson and Alzheimer's disease [22, 23]. The development of analytical protocols for detection of DA is therefore crucial for clinical diagnoses [24]. However, due to the extremely similar properties and structures, determination of DA in biological matrixes usually suffers from a series of interferences caused by other amino acids and aromatic acids, particularly ascorbic acid and uric acid [25]. Therefore, the development of highly selective analytical approaches for the determination of DA is in high demand. Our approach has very excellent sensitivity and high selectivity for the determination of DA. This sensor is also successfully applied to DA detection in complicated matrices and the possible quenching mechanism is investigated.

Experimental section

Materials and reagents

L-Cysteine (L-Cys), sodium molybdate dehydrate (Na₂MoO₄·2H₂O), aqueous ammonia (NH₃·H₂O, 28%), N-hydroxysulfosuccinimide (Sulfo-NHS), N-(3-dimethylaminopropyl)-N-ethylcarbodiimide hydrochloride (EDC), FeCl₃, KCl and CaCl₂ were bought from Sinopharm Chemical Reagent Co., Ltd. (Shanghai, China, <http://www.sinoreagent.com/>). L-Ascorbic acid (AA), dopamine

hydrochloride (DA) and uric acid (UA) were obtained from Sigma-Aldrich Chemical Co. (St. Louis, MO, USA, <http://www.sigmaaldrich.com/>). L-Epinephrine (LEE), histamine, tyramine, tryptamine, isoprenaline hydrochloride (IPE), 5-hydroxytryptamine (5-HT), L-norepinephrine (NE) and phenethylamine (PEA) were bought from Aladdin Chemistry Co., Ltd. (Shanghai, China, <http://www.aladdin-e.com/>). Tris-(hydroxymethyl) aminomethane (Tris), dopamine aptamer: 5-carbox-GTC TCT GTG TGC GCC AGA GAA CAC TGG GGC AGA TAT GGG CCA GCA CAG AAT GAG GCC C-3, 5 x TBE buffer (pH 7.9) and 3-(4,5-dimethylthiazol-2-yl)-2,5-diphenyltetrazolium bromide (MTT) were purchased from Sangon Biological Engineering Technology & Services Co., Ltd. (Shanghai, China, <http://www.sangon.com/>). MoS₂ nanosheets (1.0 mg·mL⁻¹) were bought from Nanjing XFNANO Materials Tech Co., Ltd. (Nanjing, China, <https://www.xfnano.com/>). Generuler ultra-low range molecular weight DNA ladder was bought from Thermo Scientific (shanghai, China <https://www.thermoscientific.com/>). Agarose G-10 was bought from Biowest (Biowest, France, <https://www.biowest.net/>). Purification of MoS₂ quantum dots was carried out using 1.0 kDa cutoff membranes (Amicon Ultra-4, Millipore, USA, <http://www.merckmillipore.com>). 10 mM phosphate buffered saline (PBS, pH 7.4, 2 mM KH₂PO₄, 10 mM Na₂HPO₄, 137 mM NaCl, 2.7 mM KCl). Human serum samples were supplied by the Gansu Provincial Hospital. All reagents and solvents were at least analytical-grade and directly used as received without special purification. The water used throughout all experiments was purified with a Milli-Q plus 185 equip from Millipore (Bedford, MA, USA, <http://www.millipore.com/>) system.

Instruments

Transmission electron microscopy (TEM) images were carried out by means of a Tecnai G2 TF20 transmission electron microscope (FEI, USA). Fourier transform infrared spectroscopy (FT-IR) was surveyed on an IFS120HR Fourier transform infrared spectroscopy (Bruker, German) using KBr pellets. X-Ray diffraction (XRD) patterns were acquired with an X'Pert PRO X-ray diffractometer (PANalytical, Netherlands). X-ray photoelectron spectra (XPS) analyses were observed using an ESCALAB 250Xi X-ray photoelectron spectroscope (Thermo Fisher Scientific, USA) equipped with an Al K α exciting source. Time-resolved FL spectra were collected by a time-correlated-single-photon-counting system from FL920P spectrometer (Edinburgh Instruments, U.K.). The ultraviolet-visible (UV-Vis) absorption spectra were carried out with a Lambda-35 UV-Vis spectrophotometer (Perkin Elmer, USA) with a standard 1.0-cm path length quartz cell. All FL spectra were collected by a LS-55 luminescence spectrometer (Perkin-Elmer, USA) using 5/5 nm slit width, and

equipped with a standard 1.0-cm path length quartz cell. Gel electrophoresis was carried out by a DYCP-31A Electrophoresis Cell equipped with DYY-5 Electrophoresis Power Supply (Beijing LiuYi Instrument Factory, China).

Preparation of MoS₂ QDs

QDs were prepared according to the documented hydrothermal method with minor modifications [20]. The specific synthesis details can be found in the Electronic Supporting Material (ESM).

Cytotoxicity investigation

In vitro cytotoxicity of the QDs or NSs on HeLa cells was assessed by MTT assay. Firstly, HeLa cells (100 μL) were seeded and incubated in a 96-well plate with a density of 1.0×10^4 cells $\cdot\text{well}^{-1}$ for 24 h at 37 °C in a humidified hood incubator set at 5% CO₂ atmosphere. Then, the cells were exposed to different concentrations of QDs or NSs (from 0 to 200 $\mu\text{g}\cdot\text{mL}^{-1}$) and incubated for another 24 h. Subsequently, 20 μL MTT (5 $\text{mg}\cdot\text{mL}^{-1}$ in PBS) was introduced to each well. After co-incubation for additional 4 h, the culture medium was discarded, and 150 μL dimethyl sulfoxide was added followed by vigorously shaking for 10 min in the dark. Finally, the optical density value of the each sample was recorded on a microplate reader (Thermo Scientific Multiskan GO, Finland) at a wavelength of 490 nm. Cells treated with dimethyl sulfoxide alone were used as control samples. The relative cell viability ($\text{Abs}_{\text{sample}}/\text{Abs}_{\text{control}} \times 100\%$) was evaluated by comparing their absorbance with control samples.

Fluorescence imaging of living cells

The potential for cellular imaging of the QDs was monitored by means of HeLa cells. Briefly, HeLa cells were grown on an 18-well plate and cultured in Dulbecco's modified Eagle's medium supplemented with 100 units $\cdot\text{mL}^{-1}$ penicillin, 10% fetal bovine serum and 100 units $\cdot\text{mL}^{-1}$ streptomycin in a humidified atmosphere (5% CO₂) overnight at 37 °C. Subsequently, 50 $\mu\text{g}\cdot\text{mL}^{-1}$ of QDs was mixed with the culture medium and was introduced into HeLa cells. After incubation for 3 h, the QDs loaded HeLa cells were repeatedly washed with PBS to remove the free materials. Finally, FL images of these cells were immediately captured using an Olympus Fluoview 1000 confocal laser scanning microscope.

Preparation of DA aptamer-functionalized MoS₂ QDs

The aptamer-functionalized QDs were prepared by well-established carbodiimide chemistry. Initially, EDC (2.4 mg) and NHS (3.6 mg) were added to 1.0 mL of QD solution

(1.0 $\text{mg}\cdot\text{mL}^{-1}$) and the mixture was stirred for 20 min. Subsequently, the activated QD solution was introduced into 100 μL aptamer with final concentration of 20 μM in PBS, and further incubated at 25 °C overnight. In order to remove unreacted NHS, EDC and aptamer, the final product was purified and concentrated by ultrafiltration (AmiconUltra-0.5, 20 KD, Millipore) at 4000 g for 8 min.

Gel electrophoresis

The experiments of agarose gel electrophoresis were used to identify the combination of QDs and aptamer. Briefly, Electrophoresis experiments was performed with 5.0% agarose gels by gene green nucleic acid dye staining, cast and ran at room temperature in 0.5 x TBE (pH = 7.9) buffer. Electrophoresis were carried out for 1.0 h at a constant voltage of 90 V with loading of 8.0 μL of each prepared sample into the lanes. Finally, the gel was scanned by a Quantum ST5 (Vilber, France) gel imaging system under UV light.

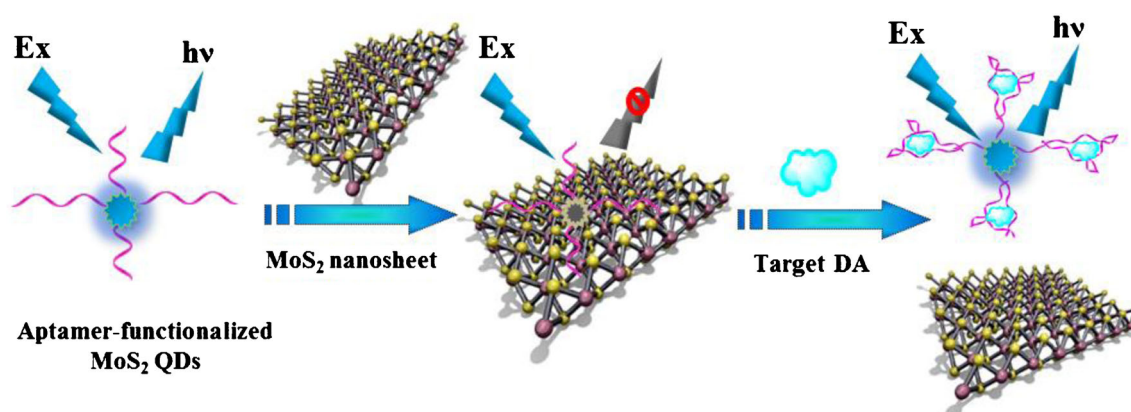
Determination of DA

DA detection was performed as follows: a certain amount of NSs (120 μL , 1.0 $\text{mg}\cdot\text{mL}^{-1}$) and 10 μL aforementioned aptamer-functionalized QDs were introduced into 820 μL of PBS. After 20 min incubation at 25 °C, 50 μL standard DA solution with different concentrations (final concentrations corresponding to 0.1, 0.2, 0.5, 0.8, 1.0, 2.0, 5.0, 10, 20, 50, 100, 200, 400, 500, 600, 800 and 1000 nM) was added into the above mixture, and allowed to further incubation at 20 °C for 30 min. Then the FL intensity was recorded in the range of 345 to 580 nm ($\lambda_{\text{ex}} = 315$ nm). The control experiments were conducted by means of measuring the FL intensity of solution after addition of the same volume of PBS rather than DA.

Results and discussion

Principle of the biosensor

Scheme 1 outlines the principle of an aptamer-functionalized QDs and NSs based turn-on FL biosensor for the analysis of DA. Firstly, DA aptamer was labeled on the surface of QDs to form an aptamer-functionalized QDs. In the absence of DA, QDs-conjugated aptamer would keep their liner structure and be adsorbed on the surface of NSs via van der Waals interaction. As a result, it brings the QDs-conjugated aptamer in close proximity to NSs (<10 nm). Furthermore, there is an overlap region between the FL emission spectrum of aptamer-functionalized QDs and the absorption spectrum of NSs (As displayed in Fig. S1). Aptamer-functionalized QDs can serve as the energy donor and recognition probe, and NSs can act as energy acceptor. Therefore, fluorescence resonance energy



Scheme 1 Schematic illustration of the aptamer-functionalized QDs and NSs based FL sensing system for DA detection

transfer (FRET) between aptamer-functionalized QDs and NSs occurs when they get close to each other, the FL of aptamer-functionalized QDs is quenched. However, after addition of DA, DA can bind with the aptamer, and then capped on the surface of QDs to form globular chain structures [25]. In this case, the complex detaches from NSs, and the FL of aptamer-functionalized QDs recovers.

Characterizations of MoS₂ nanosheets and MoS₂ quantum dots (QDs)

NSs were characterized by TEM, HRTEM, SAED, EDX and FT-IR spectrum. The details can be seen in the Electronic Supporting Material (Fig. S2 and S3). The morphology and size of our prepared QDs was examined via TEM. As illustrated in Fig. 1a, the QDs are uniform in size with spherical morphology and well monodispersed, which is consistent with previous publication [20]. As estimated from TEM, the diameters of QDs are mainly distributed in the range of 0.5 to 2.3 nm. According to the particle size distribution plot, the average particle size of the material is 1.5 nm (Fig. 1b). XRD was performed to characterize the crystal structure of QDs (Fig. 1c), four major diffraction peaks at 14.41, 32.71, 39.56 and 49.82° are readily indexed to the (002), (100), (102) and (103) planes of QDs, respectively [26]. FT-IR spectroscopy was performed to investigate the functional groups present on the surface of QDs. As displayed in Fig. 1d, the absorption peaks located at 3310, 1637, 1574 and 465 cm⁻¹ are assigned to the N–H stretching vibration, N–H bending vibration, N–H in-plane stretching vibration and Mo–S vibration, respectively [27, 28]. All the data clearly demonstrate that the amino groups are located on the surface of QDs.

XPS was used for further verify the elemental components and surface functional state the resultant QDs. As exhibited in Fig. S4, a high-resolution XPS spectrum of Mo 3d (Fig. S4A) is well-fitted into three main contributions at 232.5 eV, 228.6 eV and 226.3 eV, corresponding to Mo 3d_{3/2}, Mo 3d_{5/2} and S 2s lines, respectively [29]. The S 2p spectrum

(Fig. S4B) is deconvoluted into three peaks, S₂O₃²⁻ group (169.17 eV (2p_{1/2})), disulfides S₂²⁻ or polysulfides Sn²⁻ (164.1 eV (2p_{1/2}) and 163.5 eV (2p_{3/2})) [30].

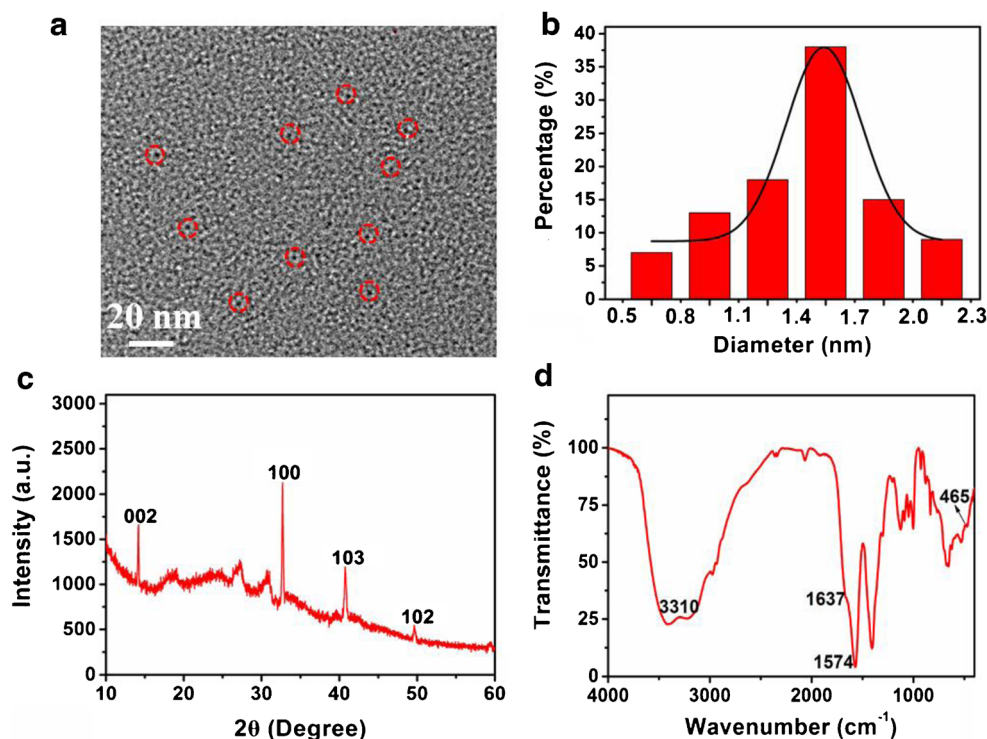
Optical properties of MoS₂ quantum dots (QDs)

The UV-vis and FL spectra were investigated to further explore the optical properties of QDs. As displayed in Fig. 2a, the QDs in aqueous solution show an intense absorption peak at 265 nm, and which is suggested to result from π - π^* transition of the aromatic sp² domains. At the same time, the QDs exhibit an emission maximum at 406 nm under 315 nm excitation. The inset of Fig. 2a shows the photographs of QD solutions on exposure to the visible and 365 nm UV light. A strong blue luminescence of QDs is easily observed with bare eyes under the irradiation at 365 nm. In addition, the emission wavelength of QDs is red shifted with the excitation wavelength increasing from 270 to 500 nm (Fig. 2b), the excitation-dependent emission wavelength and intensity behavior of QDs may be resulted from the existence of different emissive sites on the surfaces of the material or their different sizes (quantum effect).

Stability study of MoS₂ QDs

In order to study the stability of the QDs, FL intensity of the QDs toward pH value, high ionic strengths, temperature, and 315 nm light irradiation was measured. As presented in Fig. S5A, the QDs exhibit stable FL intensity in the wide range of pH 2 to 12. Fig. S5B and C display the FL intensity remained almost constant, even in concentrations of NaCl up to 1.0 M or in the temperature range from 25 °C to 45 °C. Besides, the FL intensities have little change after continuous light irradiation for 300 min (Fig. S5D). Based on the data mentioned above, we confirm that the prepared QDs possess excellent pH-stability, good salt-tolerance and outstanding photostability under the ambient environment, making them particularly suitable for biosensing and bioimaging. Furthermore, different concentrations of DA do not affect the FL intensity of QDs (Fig. S6).

Fig. 1 TEM image (a), size distribution histograms (b), XRD pattern (c) and FT-IR spectrum (d) of the synthesized QDs



Cytotoxicity and cell imaging

In order to evaluate the biocompatibility of the QDs, their toxicity to living cells was examined by a standard MTT experiments using HeLa cell line. As expected, more than 90% of cells were viable even at the concentration of QDs up to $200 \mu\text{g}\cdot\text{mL}^{-1}$ (Fig. S7, Electronic Supplementary Material). High cell viability confirm the good biocompatibility and low toxic of the QDs. Taken together, the prepared QDs give advantages of excellent stability and small size, substantially making them superior in potential bioimaging applications. Therefore, their cellular imaging capability was preliminarily carried out. As depicted in Fig. S8, after

incubated with QDs for 3 h, the HeLa cells display a significant blue FL emission when excite at wavelength of 405 nm. This result demonstrates that the QDs are taken up by the HeLa cells. In addition, QDs exhibit green, and red FL emission upon the respective excitation at 488, and 535 nm, respectively. This phenomenon is in accordance well with the excitation-independent full-colour emission character of the QDs (Fig. 2b). These images also indicate that the QDs mainly locate at cytoplasmic regions, thus suggesting that the QDs can pass through cell membranes and enter into cells. In addition, the cytotoxicity of the NSs was also evaluated. It can be found that the concentration of NSs is $100 \mu\text{g}\cdot\text{mL}^{-1}$, the cell viability is only 85.10% (Fig. S9).

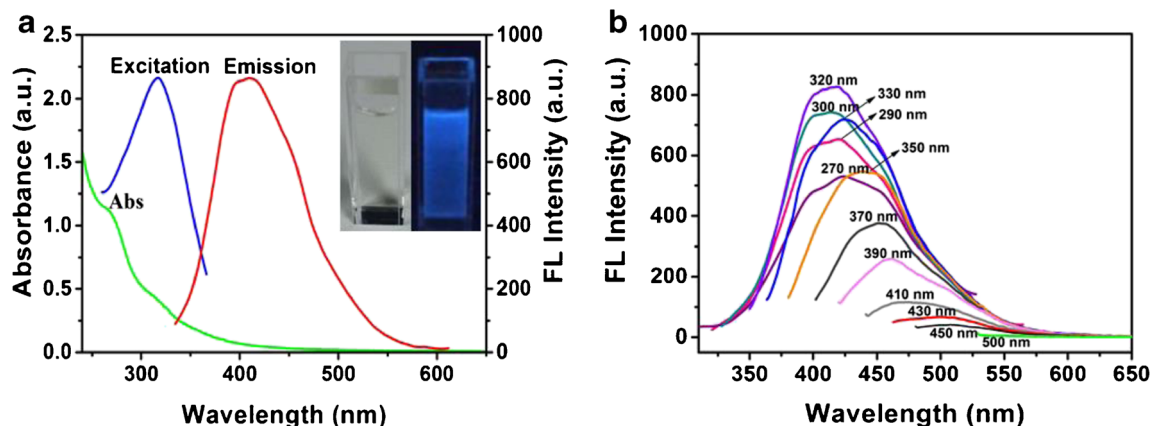


Fig. 2 (a) UV-vis and fluorescence spectra of QD solution (inset was the photographs of QD solutions under sunlight and 365 nm UV light); (b) Fluorescence emission spectra of QDs at various excitation wavelengths from 270 to 500 nm

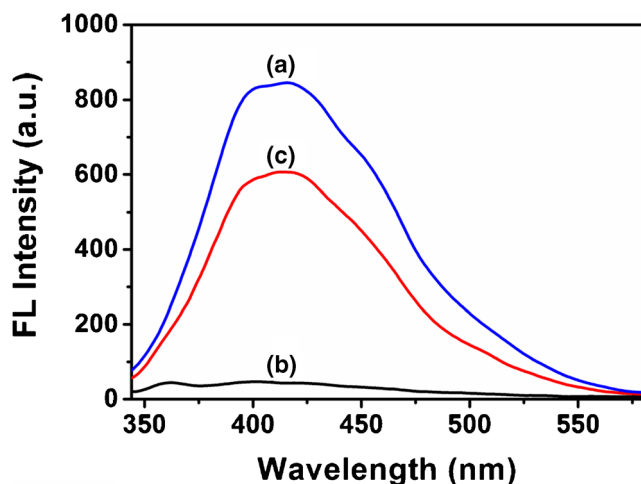


Fig. 3 FL spectra of different sample solutions at excitation/emission wavelengths of 315/412 nm: (a) aptamer-functionalized QDs; (b) aptamer-functionalized QDs + NSs; (c) aptamer-functionalized QDs + NSs + DA (1.0 μM)

The results demonstrate that QDs can be applied to imaging analysis in living cells.

Characterization of aptamer-functionalized MoS₂ QDs

The prepared aptamer-functionalized QDs was verified by agarose gel electrophoresis and FL spectrum, and the results are displayed in Fig. S10. It is found that the band of DA aptamer-functionalized QDs with a lower mobility compared with the band of pure aptamer due to the increase of mass-to-charge ratio of aptamer labeled QDs after functionalized with QDs, indicating that aptamer is successfully bonded to the surface of the QDs (Fig. S10A). In addition, the best emission peak of aptamer-functionalized QDs exhibits a slight red shift compared with the pure QDs ($\lambda_{\text{ex}} = 315 \text{ nm}$, Fig. S10B). This

is mainly due to the aptamer is covalently bound to the surface of QDs, which changes the size and surface charge of QDs.

Feasibility study

To illustrate the proof-of-principle, we investigated the FL intensity of the aptasensor strategy under different experimental conditions. As presented in Fig. 3, the aptamer-functionalized QDs exhibit strong FL intensity at 412 nm, upon the addition of NSs, the FL signal of the system decreases significantly. This phenomenon may be attributed to the superior adsorption between aptamer-functionalized QDs and NSs. However, it has a significant recovery upon addition of 1.0 μM DA. This observation indicate that the complex of aptamer-functionalized QDs and DA would detach from the surface of NSs. Thus, the fluorescent sensor might be used for the determination of DA.

Optimization of method

The following parameters were optimized: (a) concentration of aptamer; (b) incubation temperature of the combination between QDs and aptamer; (c) amount of NSs; (d) reaction temperature; (e) reaction time. Respective data and Figures are given in the Electronic Supporting Material. In short, the following experimental conditions were found to give best results: (a) optimal concentration of aptamer: 20 μM (Fig. S11A); (b) optimal incubation temperature of the combination between QDs and aptamer: 25 $^{\circ}\text{C}$ (Fig. S11B); (c) optimal amount of NSs: 120 $\mu\text{g}\cdot\text{mL}^{-1}$ (Fig. S11C); (d) optimal reaction temperature: 20 $^{\circ}\text{C}$ (Fig. S11D); (e) optimal reaction time: 30 min (Fig. S11E).

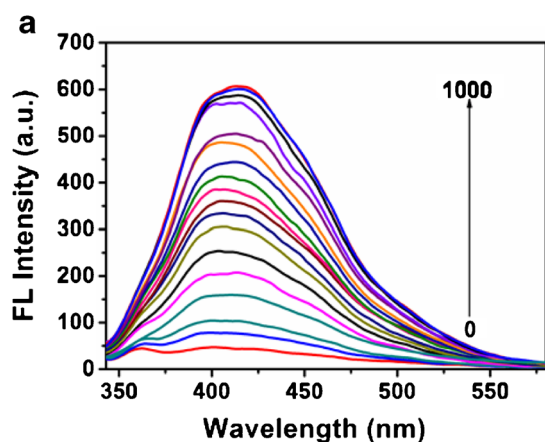
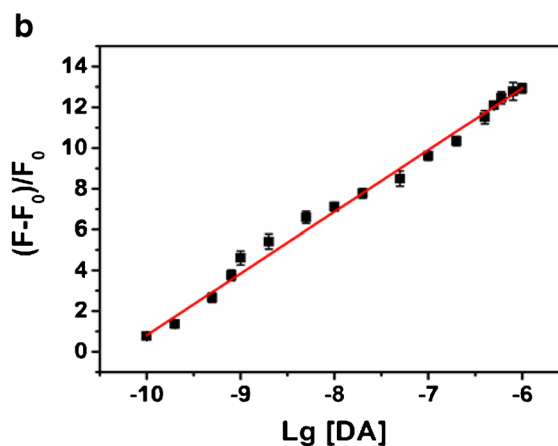


Fig. 4 (a) FL emission spectra of aptamer-functionalized QDs and NSs based FL sensing system upon the addition of various concentrations of target DA (from bottom to top, 0, 0.1, 0.2, 0.5, 0.8, 1.0, 2.0, 5.0, 10, 20, 50, 100, 200, 400, 500, 600, 800 and 1000 nM) at excitation/emission



wavelengths of 315/412 nm. (b) The liner calibration plot between relative FL intensity recovery rate $[(F-F_0)/F_0]$ at 412 nm and the logarithm of the target DA concentration. All experiments were conducted for three times under the optimum conditions

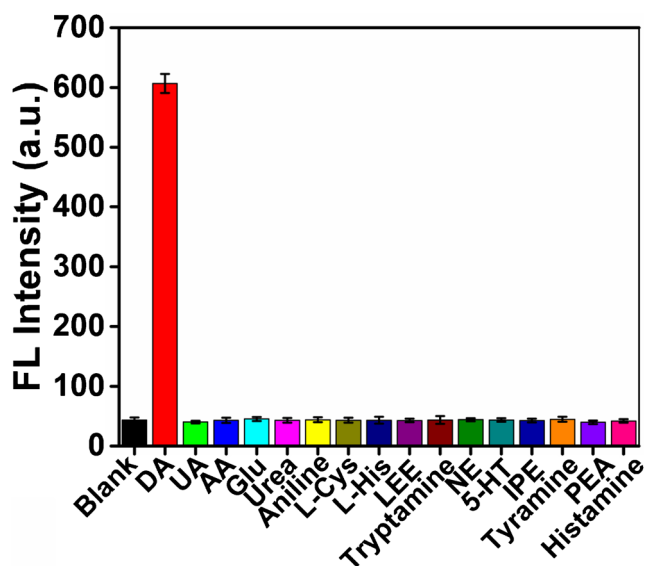


Fig. 5 FL response of aptamer-functionalized QDs and NSs based toward DA (1.0 μM) and other interferents (20-fold concentration of DA) at excitation/emission wavelengths of 315/412 nm

Detection of dopamine (DA)

As plotted in Fig. 4a, the FL intensity at 412 nm increases gradually with increasing concentrations of DA. The relative FL intensity recovery rate $[(F - F_0) / F_0]$ display a good linear relationship versus the logarithm of the target DA concentration in the range from 0.1 to 1000 nM (Fig. 4b). The linear regression can be represented as $(F - F_0)/F_0 = 31.122 + 3.031 \text{ Lg}C$ (where F_0 and F are the FL intensities of the system at 412 nm in the absence and presence of DA, respectively, C is the concentration of DA, $R^2 = 0.9956$). The limit of detection (LOD) of this assay was calculated to be 45 pM according to the rule of $3\sigma/s$ (where s is the slope of the calibration curve, σ is the standard deviation for the blank solution). Subsequently,

we compared the linear range and LOD with previous literatures on DA determination. As displayed in Table S1, the LOD of the approach is lower than or comparable to any other strategies [24, 31–34]. Furthermore, the reproducibility of this strategy was also evaluated by means of detecting 10.0 nM and 100 nM DA standard solutions. The data display that the relative standard deviations (RSDs) are all less than 4.9% ($n = 9$). These make it a competitive candidate in analytical method. Nevertheless, reducing the toxicity of NSs remains a challenge. Future work should focus on the development of low toxicity of nanomaterial for the further application in living cells.

Selectivity

Selectivity and sensitivity are the two critical factors for a successful assay protocol with potential applications in complex biological matrixes. Thus, to evaluate the selectivity of this strategy, we carried out a series of comparative experiments between the DA and the other potentially common interferences by means of the same procedures as those used for DA. The concentrations of the other potential interferences were 20 times higher than that of the target DA. As illustrated in Fig. 5, only DA induces a remarkable FL response, which clearly demonstrate that the sensor is responsive to its target molecule with outstanding selectivity.

Analytical application in real samples

To further validate the applicability of the approach for the determination of DA in real samples such as human serum and hydrochloride injection sample. Human serum samples were collected from healthy individuals. Before experiments, we prepared a series of human serum samples with different dilution rates (1:20, 1:40, 1:60, 1:80, 1:100, 1:150, 1:200), and compared the analytical performance of our method in buffer

Table 1 Determination of DA in human serum samples and DA hydrochloride injection samples

Samples	Determined (M)	Added (M)	Found (M)	RSD (% , $n = 3$)	Recovery (%)
Serum 1	Not found	5.0×10^{-7}	4.98×10^{-7}	4.5	99.6
		5.0×10^{-8}	5.02×10^{-8}	3.2	100.4
		5.0×10^{-9}	4.76×10^{-9}	2.9	95.2
Serum 2	Not found	5.0×10^{-7}	5.24×10^{-7}	4.0	104.8
		5.0×10^{-8}	4.86×10^{-8}	2.7	97.2
		5.0×10^{-9}	4.80×10^{-9}	3.4	96.0
Serum 3	Not found	5.0×10^{-7}	5.17×10^{-7}	3.1	103.4
		5.0×10^{-8}	5.23×10^{-8}	4.3	104.6
		5.0×10^{-9}	4.99×10^{-9}	2.8	99.8
DA hydrochloride injection samples	5.0×10^{-9}	1.0×10^{-9}	6.03×10^{-9}	3.6	103
		2.5×10^{-9}	7.46×10^{-9}	2.8	98.4
		5.0×10^{-9}	9.98×10^{-9}	4.1	99.6

and diluted human serum samples without the addition of DA. The results are illustrated in Fig. S12. It can be found that when the dilution ratio is up to 1:100, fluorescent intensity from the diluted human serum samples is comparable to those from buffer solution. Thus, 100-fold dilution of human serum samples were spiked with DA at different concentrations (5, 50 and 500 nM) and evaluated by the standard addition method. As displayed in Table 1, the recovery is found in the range of 96.0–104.8% with RSDs less than 4.5%, indicating that our aptasensor exhibits an acceptable accuracy and has potential practical applicability. In addition, we applied this approach to analyze DA in DA hydrochloride injection samples. The recoveries and RSD values are presented in Table 1, it can be found that the average recoveries of the DA in the range of 98.4%–103% (RSDs <5%). The above experimental results definitely demonstrate that the method can provide a promising and useful tool to detect DA in real samples.

Quenching mechanism between aptamer-functionalized MoS₂ QDs and MoS₂ nanosheets

To investigate the possible FL quenching mechanism, corresponding experiments were carried out. As displayed in Fig. S13A. The FL lifetime of the aptamer-functionalized QDs remains constant with addition of NSs and DA. Furthermore, we also investigated the Stern-Volmer quenching constants based on aptamer-functionalized QDs versus concentration of NSs at three different temperatures (288, 298, and 310 K). The well-known Stern-Volmer equation is described as $F_0/F = 1 + K_{SV} [Q]$ (where F_0 represents the steady-state FL signal in the absence of NSs, F is the steady-state FL signal in the presence of NSs, K_{SV} denotes the Stern-Volmer constant [M^{-1}], and $[Q]$ is molar concentration of NSs). It is reported that K_{SV} will increase with rising temperature in dynamic quenching effect and the reverse in static quenching effect. According to Fig. S13B, K_{SV} is inversely proportional to the temperature. The results clearly reveal that the aptamer-functionalized QDs / NSs system is a static quenching process.

Conclusions

A “turn-on” fluorescent biosensing strategy for the determination of DA is established based on aptamer-functionalized QDs and NSs. This method exhibits short detection time, high sensitivity and excellent selectivity. Simultaneously, the fluorescent sensor is applied to determine DA in complicated matrices, with satisfied results. The possible quenching mechanism involved in this work is investigated. QDs show excellent optical properties, low cytotoxicity, good stability and are

successfully applied to the FL imaging of living cell, indicating its potential application prospect in biological systems. The most important is that the sensing platform is easily used to measure other biomolecules by changing the sequence of aptamer.

Acknowledgements The authors gratefully acknowledge the financial support provided by the National Natural Science Foundation of China (Nos. 21822407, 21405163), the Funds for Distinguished Young Scientists of Gansu (1506RJDA281) and the top priority program of “One-Three-Five” Strategic Planning of Lanzhou Institute of Chemical Physics, CAS.

Compliance with ethical standards The author(s) declare that they have no competing interest.

Publisher’s Note Springer Nature remains neutral with regard to jurisdictional claims in published maps and institutional affiliations.

References

1. Ellington AD, Szostak JW (1990) In vitro selection of RNA molecules that bind specific ligands. *Nature* 346:818–822
2. Tan W, Donovan MJ, Jiang J (2013) Aptamers from cell-based selection for bioanalytical applications. *Chem Rev* 113:2842–2862
3. Huang Y, Chen J, Zhao S, Shi M, Chen ZF, Liang H (2013) Label-free colorimetric aptasensor based on nicking enzyme assisted signal amplification and DNase amplification for highly sensitive detection of protein. *Anal Chem* 88:1455–1461
4. Liu J, Lu Y (2006) Preparation of aptamer-linked gold nanoparticle purple aggregates for colorimetric sensing of analytes. *Nat Protoc* 1: 246–252
5. Song S, Wang L, Li J, Fan C, Zhao J (2008) Aptamer-based biosensors. *Trends Anal Chem* 27:108–117
6. Chen T, Shukoor MI, Chen Y, Yuan Q, Zhu Z, Zhao Z, Gulbakan B, Tan W (2011) Aptamer-conjugated nanomaterials for bioanalysis and biotechnology applications. *Nanoscale* 3:546–556
7. Kong R, Zhang X, Chen Z, Tan W (2011) Aptamer-assembled nanomaterials for biosensing and biomedical applications. *Small* 7:2428–2436
8. Lan L, Yao Y, Ping J, Ying Y (2017) Recent progress in nanomaterial-based optical aptamer assay for the detection of food chemical contaminants. *ACS Appl Mater Interfaces* 9:23287–23301
9. Zhu L, Xu G, Song Q, Tang T, Wang X, Wei F, Hu Q (2016) Highly sensitive determination of dopamine by a turn-on fluorescent biosensor based on aptamer labeled carbon dots and nano-graphite. *Sens Actuators B Chem* 231:506–512
10. Chhowalla M, Shin H, Eda G, Li L, Loh K, Zhang H (2013) The chemistry of two-dimensional layered transition metal dichalcogenide nanosheets. *Nat Chem* 5:263–275
11. Wang H, Li C, Fang P, Zhang Z, Zhang J (2018) Synthesis, properties, and optoelectronic applications of two-dimensional MoS₂ and MoS₂-based hetero structures. *Chem Soc Rev* 47:6101–6127
12. Yao Y, Tolentino L, Yang Z, Song X, Zhang W, Chen Y, Wong CP (2013) High-concentration aqueous dispersions of MoS₂. *Adv Funct Mater* 23:3577–3583
13. Li Y, Wang H, Xie L, Liang Y, Hong G, Dai H (2011) MoS₂ nanoparticles grown on graphene: an advanced catalyst for the hydrogen evolution reaction. *J Am Chem Soc* 133:7296–7299

14. Kalantar-zadeh K, Ou JZ (2016) Biosensors based on two-dimensional MoS₂. *ACS Sens* 1:5–16
15. Dai W, Dong H, Fugetsu B, Cao Y, Lu H, Ma X, Zhang X (2015) Tunable fabrication of molybdenum disulfide quantum dots for intracellular microRNA detection and multiphoton bioimaging. *Small* 11:4158–4164
16. Zhu C, Zeng Z, Li H, Li F, Fan C, Zhang H (2013) Single-layer MoS₂-based nanopores for homogeneous detection of biomolecules. *J Am Chem Soc* 135:5998–6001
17. Wang Y, Ma T, Ma S, Liu Y, Tian Y, Wang R, Jiang Y, Hou D, Wang J (2017) Fluorometric determination of the antibiotic kanamycin by aptamer-induced FRET quenching and recovery between MoS₂ nanosheets and carbon dots. *Microchim Acta* 184:203–210
18. Singh P, Gupta R, Sinha M, Kumar R, Bhalla V (2016) MoS₂ based digital response platform for aptamer based fluorescent detection of pathogens. *Microchim Acta* 183:1501–1506
19. Tang J, Huang Y, Cheng Y, Huang L, Zhuang J, Tang D (2018) Two-dimensional MoS₂ as a nano-binder for ssDNA: ultrasensitive aptamer based amperometric detection of Ochratoxin a. *Microchim Acta* 185:162
20. Wang Y, Ni Y (2015) Molybdenum disulfide quantum dots as a photoluminescence sensing platform for 2, 4, 6-trinitrophenol detection. *Anal Chem* 86: 7463–7470
21. Hu L, Zhang Q, Gan X, Ying W, Fu W (2018) Switchable fluorescence of MoS₂ quantum dots: a multifunctional probe for sensing of chromium (VI), ascorbic acid, and alkaline phosphatase activity. *Anal Bioanal Chem* 410:7551–7557
22. Zhang A, Neumeyer JL, Baldessarini RJ (2007) Recent progress in development of dopamine receptor subtype-selective agents: potential therapeutics for neurological and psychiatric disorders. *Chem Rev* 107:274–302
23. Rasheed PA, Lee JS (2017) Recent advances in optical detection of dopamine using nanomaterials. *Microchim Acta* 184:1239–1266
24. Qian T, Yu CF, Zhou X, Wu SS, Shen J (2014) Au nanoparticles decorated polypyrrole/reduced graphene oxide hybrid sheets for ultrasensitive dopamine detection. *Sens Actuators B Chem* 193: 759–763
25. Liu S, Xing X, Yu J, Lian W, Li J, Cui M, Huang J (2012) A novel label-free electrochemical aptasensor based on graphene-polyaniline composite film for dopamine determination. *Biosens Bioelectron* 36:186–191
26. Štengl V, Henych J (2013) Strongly luminescent monolayered MoS₂ prepared by effective ultrasound exfoliation. *Nanoscale* 5: 3387–3394
27. Huang KJ, Wang L, Liu YJ, Liu YM, Wang HB, Gan T, Wang LL (2013) Layered MoS₂-graphene composites for supercapacitor applications with enhanced capacitive performance. *Int J Hydrog Energy* 38:14027–14034
28. Lai L, Chen L, Zhan D, Sun L, Liu J, Lim SH, Poh CK, Shen Z, Lin J (2011) One-step synthesis of NH₂-graphene from in situ graphene-oxide reduction and its improved electrochemical properties. *Carbon* 49:3250–3257
29. Koroteev VO, Bulusheva LG, Asanov IP, Shlyakhova EV, Vyalikh DV, Okotrub AV (2011) Charge transfer in the MoS₂/carbon nanotube composite. *J Phys Chem C* 115:21199–21204
30. Turner NH, Single AM (1990) Determination of peak positions and areas from wide-scan XPS spectra. *Surf Interface Anal* 15:215–222
31. Sáenz HSC, Hernández-Saravia LP, Selva JSG, Sukeri A (2018) Electrochemical dopamine sensor using a nanoporous gold microelectrode: a proof-of-concept study for the detection of dopamine release by scanning electrochemical microscopy. *Microchim Acta* 185:367
32. Tao Y, Lin YH, Ren JS, Qu XG (2013) A dual fluorometric and colorimetric sensor for dopamine based on BSA-stabilized Au nanoclusters. *Biosens Bioelectron* 42:41–46
33. Li SJ, Deng DH, Shi Q, Liu SR (2012) Electrochemical synthesis of a graphene sheet and gold nanoparticle-based nanocomposite, and its application to amperometric sensing of dopamine. *Microchim Acta* 177:325–331
34. Khoobi A, Ghoreishi SM, Behpour M, Masoum S (2014) Three-dimensional voltammetry: a chemometrical analysis of electrochemical data for determination of dopamine in the presence of unexpected interference by a biosensor based on gold nanoparticles. *Anal Chem* 86(18):8967–8973